

Measuring and modelling optical scattering and the colour quality of white *pierid* butterfly scales.

S.M. Luke^{1,*}, P. Vukusic¹ and B. Hallam²

¹*School of Physics, University of Exeter, Exeter, EX4 4QL, UK*
²*IMERYS Minerals Ltd, Par Moor Road, Par, Cornwall, PL24 2SQ, UK*
**S.M.Luke@ex.ac.uk*

Abstract: Colouration in butterfly wings is due to the interaction of light with a covering of scales on both wing surfaces. A combination of nanostructure in the scales, which reflect or scatter light, and absorption from chemical pigments in the scales and wing substrate create the final colour appearance. We compared the wing scale morphology of the pierid butterfly *Pieris rapae* (Small White) to the reflectance spectra from its wings. Its wing scales contain a dense array of pterin pigment beads. A positive correlation between bead-array density and wing reflectance, at wavelengths where the pigment does not absorb, was identified and characterised. We observed, however, that light scatter from these beads does not account for all of the broadband light scatter observed from the wings. The rest of the scale structure plays an important role in achieving high light scatter. Furthermore, combining the underlying scattering and absorption mechanisms within the butterfly scales enabled us to quantify the optical characteristics of the samples using CIE*Lab* colour theory.

© 2009 Optical Society of America

OCIS codes: (160.1435) Biomaterials; (330.1710) Colour measurement

References and Links

1. D. L. Fox, *Animal biochromes and structural colours: physical, chemical, distributional and physiological features of coloured bodies in the animal world* (University of California Press, Berkeley, CA., 1976)
2. H. Ghiradella, "Hairs, bristles and scales" in *Microscopic anatomy of invertebrates* vol. 11A, M. Locke, ed. (Wiley-Liss: New York, 1998).
3. P. Vukusic, J. R. Sambles, and H. Ghiradella, "Optical classification of microstructure in butterfly wing-scales," *Phot. Science News* **6**, 61–66 (2000).
4. H. Ghiradella, "Structure of butterfly scales: patterning in an insect cuticle," *Microsc. Res. Tech.* **27**(5), 429–438 (1994).
5. C. W. Mason, "Structural colours in insects II," *J. Phys. Chem.* **31**(3), 321–354 (1927).
6. M. A. Giraldo, S. Yoshioka, and D. G. Stavenga, "Far field scattering pattern of differently structured butterfly scales," *J. Comp. Physiol. [A]* **194**(3), 201–207 (2008).
7. P. Vukusic, J. R. Sambles, C. R. Lawrence, and R. J. Wootton, "Quantified interference and diffraction in single *Morpho* butterfly scales," *Proc. R. Soc. Lond. B. Biol. Sci.* **266**, 1403–1411 (1999).
8. S. Kinoshita, S. Yoshioka, and K. Kawagoe, "2002 "Mechanisms of structural colour in the *Morpho* butterfly: cooperation of regularity and irregularity in an iridescent scale," *Proc. R. Soc. Lond. B. Biol. Sci.* **269**(1499), 1417–1421 (2002).
9. R. B. Morris, "Iridescence from diffraction structures in the wing scales of *Callophrys rubi*, the Green Hairstreak," *J. Entomol. Ser. A* **49**, 149–154 (1975).
10. P. Vukusic, and J. R. Sambles, "Photonic structures in biology," *Nature* **424**(6950), 852–855 (2003).
11. K. Kertész, Z. Bálint, Z. Vértésy, G. I. Márk, V. Lousse, J. P. Vigneron, M. Rassart, and L. P. Biró, "Gleaming and dull surface textures from photonic-crystal-type nanostructures in the butterfly *Cyanophrys remus*," *Phys. Rev. E Stat. Nonlin. Soft Matter Phys.* **74**(2 Pt 1), 021922 (2006).
12. R. O. Prum, T. Quinn, and R. H. Torres, "Anatomically diverse butterfly scales all produce structural colours by coherent scattering," *J. Exp. Biol.* **209**(Pt 4), 748–765 (2006).
13. H. Ghiradella, D. Aneshansley, T. Eisner, R. E. Silberglied, and H. E. Hinton, "Ultraviolet reflection of a male butterfly: interference color caused by thin-layer elaboration of wing scales," *Science* **178**(4066), 1214–1217 (1972).
14. F. E. Lutz, "Invisible colors of flowers and butterflies," *J. Am. Mus. Nat. Hist.* **33**, 565–576 (1933).

15. K. Makino, K. Satoh, M. Koike, and N. Ueno, "Sex in *Pieris rapae* L. and the pteridin content of their wings," *Nature* **170**(4335), 933–934 (1952).
16. B. Wijnen, H. L. Leertouwer, and D. G. Stavenga, "Colors and pterin pigmentation of pierid butterfly wings," *J. Insect Physiol.* **53**(12), 1206–1217 (2007).
17. J. M. Kolyer, and A. Reimschuessel, "Scanning electron microscopy on wing scales of *Colias eurytheme*," *J. Res. Lepidoptera* **8**, 1–15 (1970).
18. N. Yagi, "Note of electron microscope research on pterin pigmentation in pierid butterflies," *Annot. Zool. Jpn.* **27**, 113–114 (1954).
19. N. I. Morehouse, P. Vukusic, and R. L. Rutowski, "Pterin pigment granules are responsible for both broadband light scattering and wavelength selective absorption in the wing scales of pierid butterflies," *Proc. R. Soc. Lond. B. Biol. Sci.* **274**(1608), 359–366 (2007).
20. R. L. Rutowski, J. M. Macedonia, N. I. Morehouse, and L. Taylor-Taft, "Pterin pigments amplify iridescent ultraviolet signal in males of the orange sulphur butterfly, *Colias eurytheme*," *Proc. R. Soc. Lond. B. Biol. Sci.* **272**(1578), 2329–2335 (2005).
21. D. G. Stavenga, S. Stowe, K. Siebke, J. Zeil, and K. Arikawa, "Butterfly wing colours: scale beads make white pierid wings brighter," *Proc. R. Soc. Lond. B. Biol. Sci.* **271**(1548), 1577–1584 (2004).
22. D. J. Kemp, P. Vukusic, and R. L. Rutowski, "Stress-mediated covariance between nano-structural architecture and ultraviolet butterfly coloration," *Funct. Ecol.* **20**(2), 282–289 (2006).
23. Y. Obara, and T. Hidaki, "Recognition of the female by the male, on the basis of ultra-violet reflection, in the white cabbage butterfly, *Pieris rapae crucivora* Boisduval," *Proc. Jpn. Acad.* **44**, 829–832 (1968).
24. Y. Obara, and M. E. N. Majerus, "Initial mate recognition in the British cabbage butterfly, *Pieris rapae rapae*," *Zoolog. Sci.* **17**(6), 725–730 (2000).
25. P. Vukusic, B. Hallam, and J. A. Noyes, "Brilliant whiteness in ultrathin beetle scales," *Science* **315**(5810), 348 (2007).
26. S. Yoshioka, and S. Kinoshita, "Structural or pigmentary? Origin of the distinctive white stripe on the blue wing of a *Morpho* butterfly," *Proc Biol Sci* **273**(1583), 129–134 (2006).
27. P. Kubelka, and F. Munk, "Ein Beitrag zur Optik der Farbanstriche," *Z. Tech. Phys* **12**, 593–601 (1931).
28. N. Pauler, *Paper Optics* (AB Lorentzen & Wettre, Kista, Sweden, 1998).
29. J. A. Endler, "On the measurement and classification of colour in studies of animal colour patterns," *Biol. J. Linn. Soc. Lond.* **41**(4), 315–352 (1990).
30. M. F. Land, "The physics and biology of animal reflectors," *Prog. Biophys. Mol. Biol.* **24**, 75–106 (1972).
31. J. A. Noyes, P. Vukusic, and I. R. Hooper, "Experimental method for reliably establishing the refractive index of puprestid beetle exocuticle," *Opt. Express* **15**(7), 4351–4358 (2007).
32. P. Lewicki, and T. Hill, "Statistics methods and application" (StatSoft, Tulsa, OK., 2007) <http://www.statsoft.com/textbook/stathome.html>.
33. M. A. Giraldo, and D. G. Stavenga, "Sexual dichroism and pigment localization in the wing scales of *Pieris rapae* butterflies," *Proc. R. Soc. Lond. B. Biol. Sci.* **274**(1606), 97–102 (2007).
34. M. A. Giraldo, and D. G. Stavenga, "Wing coloration and pigment gradients in scales of pierid butterflies," *Arthropod Struct. Dev.* **37**(2), 118–128 (2008).
35. M. Gates, "The Chemistry of the Pteridines," *Chem. Rev.* **41**(1), 63–95 (1947).
36. W. B. Watt, "Pteridine components of wing pigmentation in the butterfly *Colias eurytheme*," *Nature* **201**(4926), 1326–1327 (1964).
37. D. G. Stavenga, M. A. Giraldo, and B. J. Hoenders, "Reflectance and transmittance of light scattering scales stacked on the wings of pierid butterflies," *Opt. Express* **14**(11), 4880–4890 (2006).
38. S. Yoshioka, and S. Kinoshita, "Single-scale spectroscopy of structurally colored butterflies: measurements of quantified reflectance and transmittance," *J. Opt. Soc. Am. A* **23**(1), 134–141 (2006).
39. ISO2470, 1999.
40. Y. Obara, "Studies on the mating behavior of the white cabbage butterfly, *Pieris rapae crucivora* Boisduval. III. Near-ultraviolet reflection as the signal of intraspecific communication," *Z. Vgl. Physiol.* **69**(1), 99–116 (1970).
41. R. L. Rutowski, "The use of visual cues in sexual and species discrimination by males of the small sulphur butterfly *Eurema lisa* (Lepidoptera, Pieridae)," *J. Comp. Physiol.* **115**(1), 61–74 (1977).
42. P. Vukusic, J. R. Sambles, and C. R. Lawrence, "Structurally assisted blackness in butterfly scales," *Proc. R. Soc. Lond. B. Biol. Sci.* **271**(0 suppl.), S237–S239 (2004).

1. Introduction

Butterflies are known to produce some of the most vivid colours in nature. This has attracted a wealth of research interest to determine the mechanisms responsible for such colour diversity. Invariably, these colours are due either to pigments that absorb light over a limited wavelength range; to microstructures that scatter light strongly over a specific wavelength range; or to a combination of both [1–3].

Research into the optical properties of butterfly wings has revealed many of the structural forms responsible for the selective colour reflection associated with their wing scales [2–4].

For instance, multilayer interference is associated with the mechanism of colour production in *Urania* moths [5, 6]; concurrent multilayer interference and diffraction is attributed to the diffuse iridescent appearance of *Morpho didius* [7, 8]; Bragg scattering of narrow wavelength bands is the mechanism responsible for the colour of many butterflies with three dimensionally ordered intra-scale structures [9–12].

Most species of Lepidoptera have a bilayer of scales on both dorsal and ventral wing surfaces. Each scale is a flattened projection of cuticle from an epidermal cell in the wing surface [4]. Generally it is these scales that are responsible for wing colouration, although pigmentation of the wing substrate may also affect the colour of the wing. Although there are many variations in wing scale morphology, they generally have the same fundamental structure. Ridges are observed to run along the longitudinal length of the scales and these are connected by crossribs. This creates a two dimensional lattice structure above the scale interior [2]. Butterflies of the family Pieridae exhibit a dense array of ellipsoidal beads within their wing scales; these beads are suspended from the ridges and crossribs and hang down into the scale interior [2, 13]. Male pierids generally display a much denser bead-array within their wing scales than females.

Wing colouration of pierid butterflies has long been of interest to researchers. Prior to the invention of the scanning electron microscope (SEM) the identification of wing scale microstructure was not possible. Early work, therefore, concentrated on macroscopically measurable optical properties, revealing the strong ultraviolet absorption by pterin pigments and a marked gender difference in optical properties [14, 15]. Pterins are a class of pigments with differing absorption properties, for instance, leucopterin absorbs exclusively in the UV whereas erythropterin absorbs up to a wavelength of 500nm [16]. Both leucopterin and erythropterin have been identified in pierid butterfly wing scales.

Early SEM studies allowed microscopic analysis of the wing scales and revealed the extent of the presence of ellipsoidal beads suspended from the scale ridges and crossribs [17]. Later research concluded that the pterin pigment was isolated within these dense scale bead arrays [18–20]. Recent work by Stavenga et al. has suggested that these beads also play an important role in enhancing broadband light scatter from wing scales [21]. Morehouse *et al.* found evidence of this when they detected a correlation between pterin bead-array density and absolute reflectance for the pierid butterfly *Pontia protodice* [19].

Wing colour can play an important role in butterfly species' behaviour, particularly in the case of mate selection. For example, the wing colour of the male pierid *Colias eurytheme* is associated with the quality of the scale microstructure and gives an indication of the biological fitness of the butterfly [19, 22]. Female Japanese cabbage white butterflies, *Pieris rapae crucivora* use their wing colouration to help elicit a mating response from males [23]. Female *P. rapae crucivora* display significant wing reflectance at both visible and ultraviolet (UV) wavelengths [24], whereas male *P. rapae crucivora* display very little UV wing reflectance. It has been suggested that this significant UV-visible contrast between sexes plays a fundamental role in initial mate selection [24].

The wings of pierid butterflies vary in colour [13, 16]. However, it is particularly the white winged pierids that are the subject of this study. Bright whiteness is relatively rare in insects. The process of creating the appearance of whiteness requires a random distribution of microstructure, which scatters all visible wavelengths simultaneously with comparable efficiency [25]. This process is in contrast to that associated with the scattering of narrow bands of wavelength that arises from highly periodic microstructures in other butterfly systems, for instance the butterfly *Morpho rhetenor* employs a highly periodic microstructure to generate its bright blue appearance [7]. In addition to the presence of randomly distributed microstructure, whiteness is also generally, but not always, associated with the absence of absorbing pigmentation [1,26, unpublished data].

In this study we use SEM imaging and reflectance spectrophotometry to characterise the relationship between the wing reflectance and colour quality of the male *P. rapae* butterfly

and the density of their wing scale pterin bead-array. We detail a new technique for measuring approximate light scatter coefficients on biological species and use this technique to provide a thorough analysis of bead removal and its impact on the ability of the structure to scatter light. This highlights the importance of other parts of the scale structure for strong optical scatter; we use finite element modelling to further investigate this result. We also use quantitative colour theory to evaluate the impact of modify the scale structure.

2. Materials and methods

2.1 Animals

Male *P. rapae* specimens from a bred colony in Warwickshire, UK, were obtained from *World Wide Butterflies* (www.wwb.co.uk).

2.2 Reflectance spectrophotometry

Reflection spectra were collected using an industrial standard Datacolor ELREPHO[®] 3300 spectrophotometer with D65/10 illumination. The system allows reflectance, relative to a white reflectance standard, to be measured over a working wavelength range of 400-700 nm.

A total of 40 wing samples, previously removed from purchased specimens were mounted on a black plastic backing. A 6 mm diameter aperture was used on the spectrophotometer allowing the measurement of many different sections of each wing sample. Five reflectance spectra were taken from the dorsal surface of each wing sample in order to account for variation in reflectance across the wing. This process was repeated on all samples after the extraction of pterin beads.

2.3 Scattering Coefficient – Kubelka-Munk theory

The same spectrophotometer was employed to collect reflectance spectra over a variety of different, well-characterised backgrounds from light grey through to black ([RGB] = [220, 220, 220], [160, 160, 160], [0, 0, 0]). Again a 6 mm illumination aperture was employed. Using the difference in reflectance from the sample mounted on the backgrounds of different reflectance enables the amount of light scattered (S) and absorbed (K) to be de-convolved from the reflected signals using basic Kubelka-Munk theory [27, 28]. Whilst strictly only applicable to homogeneous surfaces, Kubelka-Munk theory can be used in the case of the butterfly wings as we are averaging over a large area (137 mm²) and recording an integrated response from all the local inhomogeneous regions within the illumination aperture. In order to process the required calculations, the mass per unit area in g/m² of the test material had to be quantified. Therefore, each wing sample was weighed on a milligram scale top-pan balance (Sartorius Analytic A120S), allowing measurement to an accuracy of 1×10^{-4} g. Each wing sample was then imaged using a digital camera and the digital images are processed using IMAGEJ software (NIH freeware, <http://rsb.info.nih.gov/ij/>) in order to ascertain the sample area.

2.4 Whiteness quality measurement

The spectrophotometer used was designed specifically to measure the reflectance of white surfaces. It also permits the whiteness quality, luminosity and yellowness to be quantified, in addition to the calculation of the surfaces' colour coordinates. These are variables associated with the wings' overall colour quality that are understood to be linked to the pterin bead array density. Rutowski *et al.* [20], for instance, used Endler's segment classification method [29], to quantify the hue of the coloured wings of the butterfly *Colias eurytheme*. They found that the presence of pterins increases UV/visible colour contrast during wing movement. Here we used the CIE*Lab* colour space to quantify the whiteness, brightness and colour quality dependence of *P. rapae* wings on their wing scale pterin bead-array densities. It must be noted that the CIE*Lab* colour system is based on human colour perception. While it is not

appropriate for analysis of how conspecific species perceive wing colour, *CIELab* nonetheless provides crucial insight and information regarding the colour properties of the wing. Here we analyse wing colour quality in the context of learning from the optical systems with a view to future technological applications, such as specialised paper coatings.

CIELab is a three dimensional colour space consisting of a black-white axis (L^*), a red-green axis (a^*) and a yellow-blue axis (b^*). L^* is the luminosity which ranges from 0 to 100. The hue of the colour is determined by a^* and b^* ; a^* ranges from -128 (pure green) to $+128$ (pure red). Similarly b^* ranges from -128 (pure blue) to $+128$ (pure yellow). The centre of this colour space is defined as the neutral point with a^* and b^* equal to zero. Perfect white in *CIELab* space is associated with values for (L^* ; a^* ; b^*) of (100; 0; 0) [28].

In this investigation, the spectrophotometer measured the reflectance spectrum in three colour ranges. These values are used to calculate the tristimulus values X, Y, and Z. The tristimulus values correspond to the amount of red, green and blue light measured. They are values calculated by summing the weighted spectral reflectances. The specific weighting factors are products of the colour matching functions and the spectral energy distribution of the illuminant [28]. The luminosity and colour coordinates L^* , a^* and b^* may then be calculated from the tristimulus values by:

$$L^* = 116 \left(\frac{Y}{Y_n} \right)^{1/3} - 16, \quad (2.1)$$

$$a^* = 500 \left(\left(\frac{X}{X_n} \right)^{1/3} - \left(\frac{Y}{Y_n} \right)^{1/3} \right), \quad (2.2)$$

$$b^* = 200 \left(\left(\frac{Y}{Y_n} \right)^{1/3} - \left(\frac{Z}{Z_n} \right)^{1/3} \right), \quad (2.3)$$

where X_n , Y_n and Z_n are the coordinates of the neutral (white) point, and represent the tristimulus values for the light source or a perfect reflecting diffuser [28].

2.5 Pterin bead extraction

The effect of pterin beads on the optical properties of *P. rapae* wings was studied by comparing the spectral properties of the wings before and after removal of the beads, following the method described by Rutowski *et al.* [20]. The wings were detached from the specimens and soaked until saturated in 70% isopropyl alcohol, then immersed in ammonium hydroxide (NH_4OH) solutions of varying concentrations for time periods ranging from five seconds to five hundred seconds. This process has previously been shown to remove the wing scale pterin beads of pierid butterflies whilst leaving the main wing scale structure intact [20]. Initially a concentration of 1% NH_4OH was used, based on the concentrations used by Rutowski *et al.* [20] and Morehouse *et al.* [19]. However, concentrations of 0.65%, 0.25%, 0.1% and 0.05% NH_4OH were also used allowing the pterin beads to be removed in a slower, more controlled manner.

2.6 SEM measurements of bead size and bead-array density

Wing scales were removed from the dorsal surface of each wing sample prior to and after treatment with NH_4OH solutions and were placed on SEM stubs. The stubs were sputter coated with a thin layer (typically 2-4 nm) of gold palladium and imaged using a SEM (FEI Novalab 600 Dual beam). To identify and measure the scale features, the digital SEM images were analysed using IMAGEJ software. The bead-array density was calculated by counting

the number of beads over a large intra-scale area for a significant sample of scales (typically sample size > 10).

2.7 Theoretical modelling

All theoretical modelling was carried out using the RF module of the commercial finite element modelling package *Comsol Multiphysics*TM. Models were created using the built-in design package, using dimensions measured directly from SEM image analysis.

In order to identify the contribution of each of the scale components to the optical properties of the scale we built up our model in stages, adding further detail at each stage. Initially individual pterin beads and arrays of pterin beads were modelled separately as both solid ellipsoids and hollow ellipsoids with a skin thickness of 8 nm. The hollow bead dimensions were based on measurements taken from transmission electron microscope images by Stavenga *et al.* [21]. In the absence of available optical data describing the refractive index of pterin, a value of 1.56, identical to that of generic cuticle [30, 31] was used. The models incorporating hollow beads were modelled with air filled cavities inside each bead (refractive index $n = 1.0$).

Scattering coefficient (S) calculations indicated quantitatively that non-bead intra-scale structures contribute significantly to the optical scatter observed. This was previously shown qualitatively by other work [18, 21]. Our modelling of non-bead structures focussed on the lower substrate of the scales. To replicate this basal layer, a 95 nm thick substrate (Refractive index $n = 1.56$) was added 800nm below the centre of the beads, these dimensions were measured from SEM images.

To model the disorder of the pterin bead array accurately a real region of wing scale structure was digitally replicated. To this end, a small section of a *P. rapae* scale was imaged by SEM (Fig. 3(a)). The full three-dimensional model of this region was found to be prohibitively large for use with the finite element method at the highly resolved mesh size required. Therefore ten two dimensional cross sections were sampled in planes through the image; this yielded ten different model geometries, with varying contributions of bead array disorder. These ten modelled planes are represented by dashed white lines in Fig. 3(a). Some simplifying assumptions were applied; each bead was identical with dimensions of 525 nm × 170 nm (long and short axis) and had their long axis vertically aligned. Any real variation away from these assumptions would result in increased relative disorder and subsequent increase in optical scatter. The theoretical values of optical scatter from each of the ten cross sections were averaged. This removed any dominant effects associated with the presence of short-range periodicity in any of the ten cross sections. Furthermore, it also incorporates the spatial position disorder of the individual beads in the array.

To model the effect of the pterin pigmentation the UV-visible absorption profile of representative pigmentation, leucopterin was incorporated. Leucopterin was chosen as our spectroscopy results indicated that it is the most likely pterin present in the wings of *P. rapae*. The absorption profile of leucopterin was used to calculate an approximate wavelength dependent κ profile [16], where κ is the extinction coefficient, i.e. the imaginary part of the complex refractive index of the material. This was then approximated with a Boltzmann function such that κ could be included in the model as:

$$\kappa = \frac{(0.332 - 6.41 \times 10^{-4})}{1 + \exp((\lambda - 410.6 \times 10^{-9}) / 10.20 \times 10^{-9})} + 6.41 \times 10^{-4}. \quad (2.4)$$

3. Results

3.1 Wing scale morphology

The general structure and wing morphology of both dorsal and ventral surfaces of the wings of *P. rapae* (Fig. 1(a)) were investigated with a SEM. Typically, the scales that cover the

wings (Fig. 1(b)) measure approximately $150\ \mu\text{m} \times 60\ \mu\text{m}$ and are in the thickness range of $2 - 3\ \mu\text{m}$. The upper surface (superstrate) of the scales is highly structured with a regular

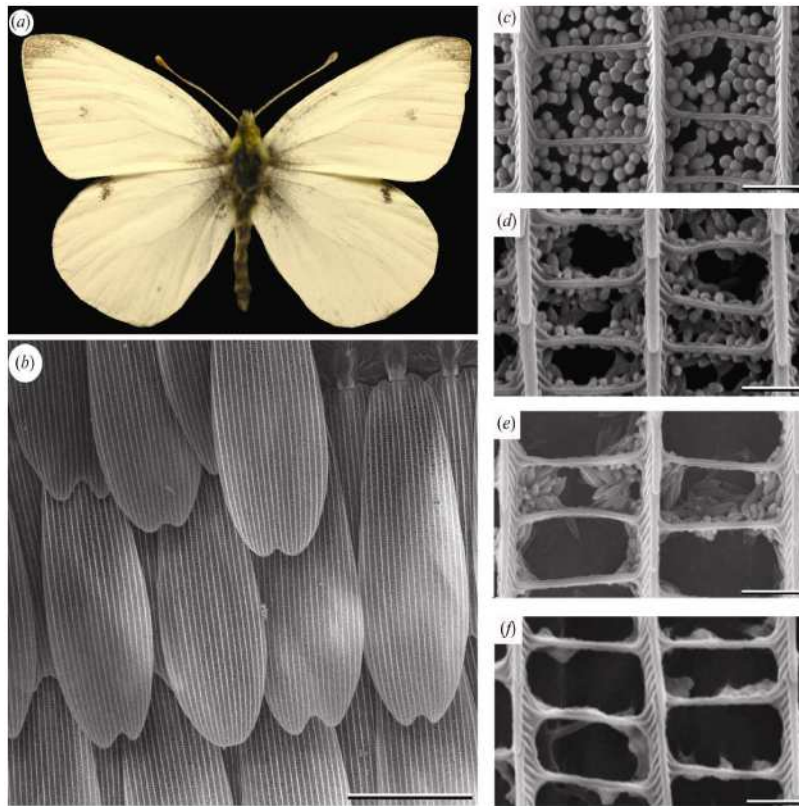


Fig. 1. (a) A male Small White, *Pieris rapae*, butterfly. (b) Scales on the wings of the *P. rapae*. The scales have scalloped ends and are positioned in overlapping rows. (c-f) SEM images of dorsal wing scales from a male *P. rapae* after exposure to increasing immersion times in 1% ammonium hydroxide (NH_4OH). (c) Untreated scale, (d) 10 seconds immersion, (e) 30 seconds immersion and (f) 1-minute immersion. Scale bars: (a) 1 cm, (b) $50\ \mu\text{m}$ and (c-f) $1\ \mu\text{m}$.

arrangement of longitudinal ribs connected by a series smaller crossribs (Fig. 1(c)). The ribs have a spacing of approximately $2.3 \pm 0.1\ \mu\text{m}$ with the crossribs separated by $0.95 \pm 0.15\ \mu\text{m}$. A disordered array of ellipsoidal shaped beads is suspended from the ribs and crossribs, hanging down into the scale interior. More detailed SEM imaging of fractured scale regions reveals that the ellipsoidal beads have typical dimensions of $525 \pm 90\ \text{nm}$ long axis and $170 \pm 15\ \text{nm}$ short axis. The lower surface of the scales (substrate) is a relatively flat surface *ca.* $95\ \text{nm}$ thick, situated approximately $1\ \mu\text{m}$ below the pterin bead-array.

3.2 Effect of pterin bead array density on wing reflectance

Bead array density was calculated for all wing samples after immersion in NH_4OH solutions, following the procedure described by Rutowski *et al.* [20]. An increase in concentration of NH_4OH solution leads to a more rapid removal of the pterin beads (Fig. 2(a)). Bead-array density was found to be negatively correlated with immersion time. In line with the approach taken by Morehouse *et al.* [19], we analysed the correlation between immersion time and other variables. For all data sets the statistical *p*-value [32] showed that immersion time in NH_4OH was significant in explaining remaining pterin bead array density. (With reference to Fig. 2(a): in 1.00% NH_4OH , $r^2 = 0.99$, $p = 0.00028$; in 0.65% NH_4OH , $r^2 = 0.97$, $p = 0.0011$; in 0.25% NH_4OH , $r^2 = 0.97$, $p = 0.0011$; in 0.10% NH_4OH , $r^2 = 0.92$, $p = 0.0015$; in 0.05%

NH_4OH , $r^2 = 0.95$, $p = 0.00013$.) Beyond an NH_4OH solution concentration of 0.25%, there is no change in the pterin bead removal rate. However, up to this concentration there appears to be a bead removal rate that can be controlled with NH_4OH solution concentration.

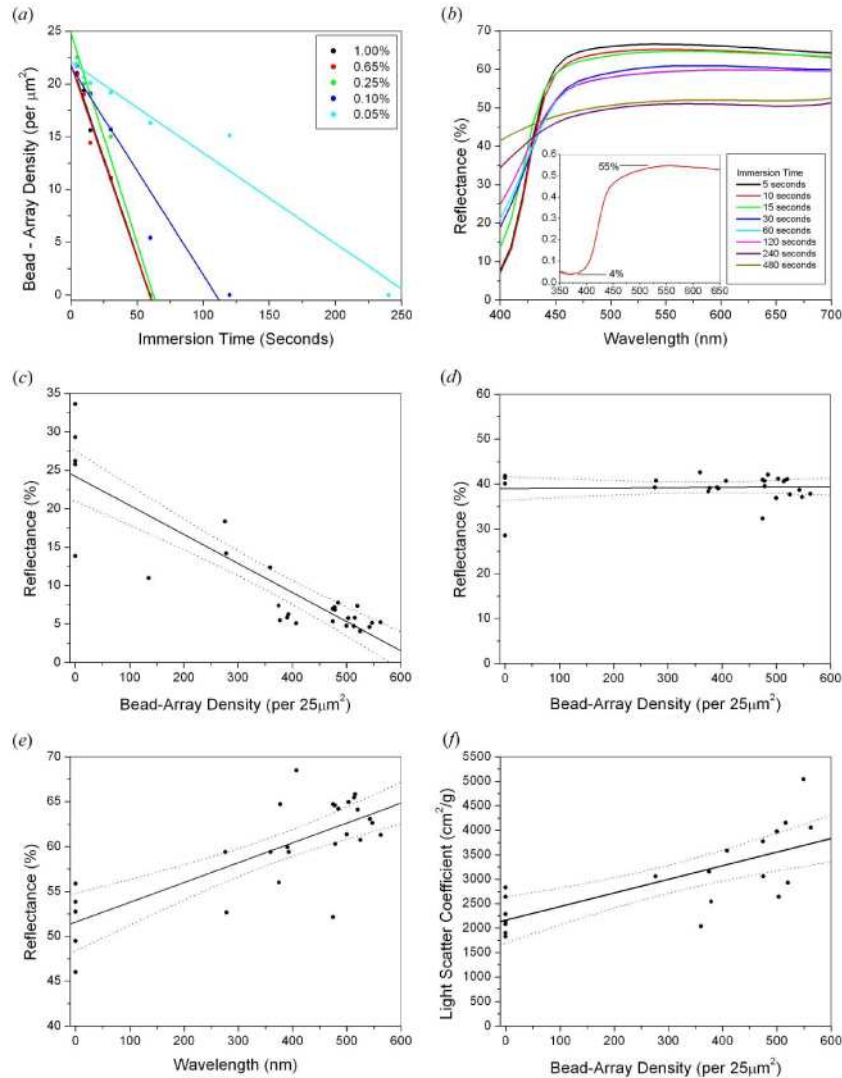


Fig. 2. (a) Pterin bead-array density decreases linearly with immersion time; increasing the NH_4OH concentration increases the bead removal rate. (b) Reflectance for male dorsal *P. rapae* wings. (c) At 400 nm the reflectance increases as pterin beads are removed. (d) At 430 nm pterin absorption offsets scattering from the beads and results in no discernable change in reflectance. (e) Wing reflectance at 550 nm; at longer wavelengths, reflectance decreases as scattering centres (pterin granules) are removed. (f) Light scattering coefficient (S); as pterin beads are removed, the amount of light scattered from the wing decreases.

Removal of the pterin beads had two principal effects on wing reflectance (Fig. 2(b)). At short wavelengths (400-450 nm) reflectance increased from *ca* 8% for untreated wings to *ca*. 40% for wings from which all beads had been removed (reflectance measured relative to a Barium Sulphate white reflectance standard). This is entirely expected due to the associated pterin absorption. Conversely, reflectance at longer wavelengths was reduced from *ca*. 65% (untreated wings) to *ca*. 50%. This is symptomatic of the decrease in scattering due to the absence of pterin beads.

Previously, it has been suggested that the density of pterin bead-array might influence the amount of light scattered by the scales [19, 21, 33, 34]. In this study, bead array densities for scales treated in NH_4OH solution were regressed against total wing reflectance. At shorter wavelengths, where UV absorption by the pterin is significant, there is a strong negative correlation between total scale reflectance and bead-array density ($r^2 = 0.72$, $p < 0.001$) (Fig. 2(c)). At a wavelength of *ca.* 430 nm there appears to be a critical point where the reduced optical reflectance from the pterin beads is offset by the reduction in optical absorption. At approximately this wavelength, the NH_4OH solution treatment has little effect on scale reflectance (Fig. 2(d)). This is consistent with expectation; the gradient of the fit line cannot be statistically distinguished from zero ($r^2 = 0.02$, $p = 0.72$). At longer wavelengths ($\lambda > 430$ nm), where optical scattering rather than absorption dominates, there is a positive correlation between bead-array density and wing reflectance (Fig. 2(e)). For instance, at 550 nm, bead-array density strongly accounts for reflectance (550 nm; $r^2 = 0.57$, $p < 0.001$). As expected, the reflectance data produced here indicates that the density of the pterin bead-array on *P. rapae* wing scales is a significant factor in explaining wing reflectance. This is consistent with the experimental data of Morehouse *et al.* [18] and the work of Stavenga *et al.* [21].

3.3 Effect of pterin bead array density on wing scattering coefficient

Calculation of the light scatter coefficient (S) and absorption coefficient (K) of the wing sample enables their optical response to be understood more clearly. This is critical, because these are two of the important factors that govern the reflectance of the sample and that contribute to its perceived colour [28].

Figure 2(f) shows the relationship between light scatter coefficient and bead-array density for male *P. rapae* wing scales. Light scatter was observed to increase with increasing density within the bead-array; this confirmed that the beads are a major contributor to sample reflectance through enhanced light scatter. The relationship appears to follow a linear trend with bead-array density ($r^2 = 0.54$, $p < 0.001$), although this is based on a small sample size of approximately 20 with natural biological variation between samples.

The graph also shows that the light scatter coefficient (S) of the wing does not tend to zero when all the beads have been removed. This shows quantitatively that non-bead intra-scale structures contribute significantly to the optical scatter observed. This has been suggested previously by other work [19, 21]. The remaining light scatter must be a result of the bi-grating-like superstrate, or the planar substrate of the wing scale. In order to investigate this further, detailed modelling of the scale components was carried out.

3.4 Theoretical modelling of pterin beads

Initial modelling work focussed on accurately replicating the pterin beads. Models using solid beads, rather than hollow beads, consistently yielded greater scattered intensities. The scattered intensity from the hollow beads was calculated to be several orders of magnitude smaller than that of the scattered intensity from the solid beads. The scattered intensity from the hollow beads was found to be too low to emulate our experimentally collected data. Therefore all subsequent modelling was carried out using solid pterin beads.

Our modelled scattering patterns are presented in Figs. 3(b) – (f), where the colour scale represents the scattered power density. This was calculated as the Poynting vector of the scattered electric field at a circular radiation boundary several wavelengths from

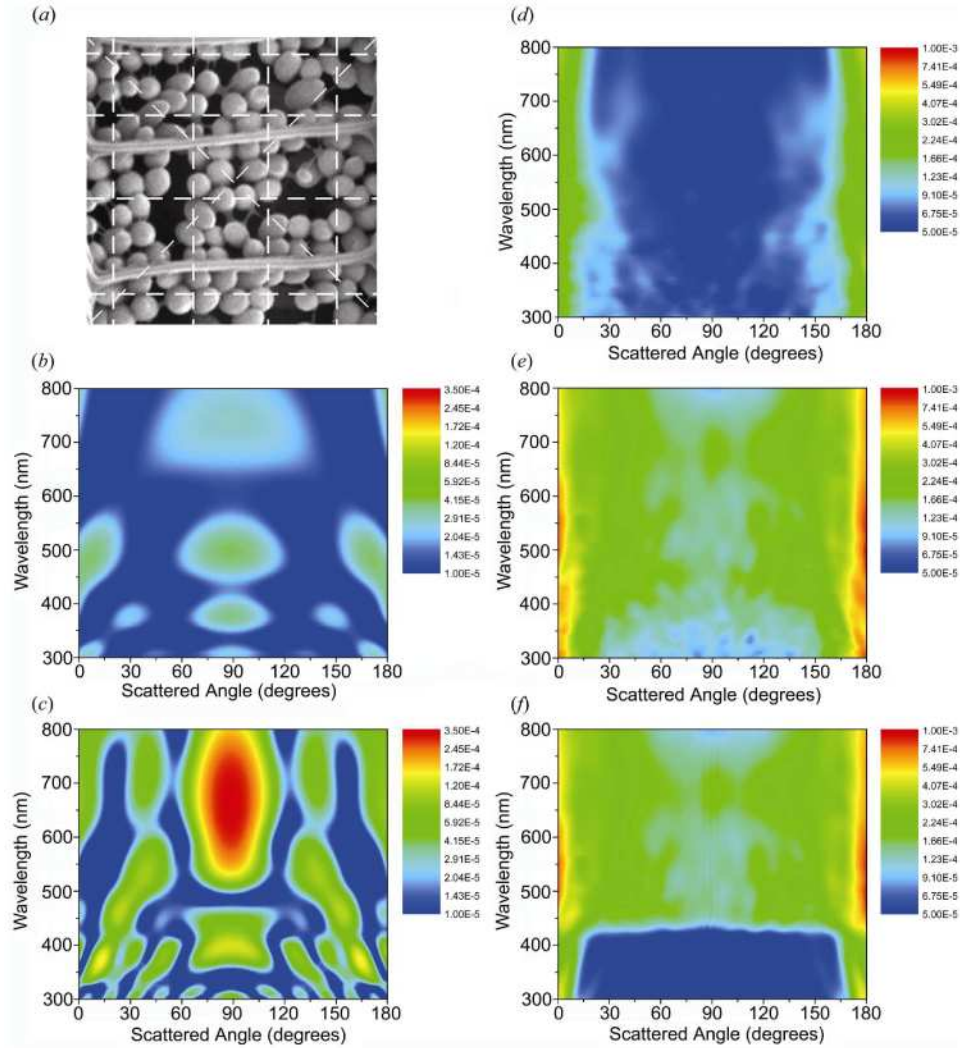


Fig. 3. (a) SEM image of the $2 \mu\text{m} \times 2 \mu\text{m}$ *P. rapae* intra-scale region used to generate finite element model geometries. Analysing the position and size of each bead along the ten white dotted lines created ten model scale sections. The power density back scattered into the dorsal hemisphere from each of the ten sections was calculated from the models and a mean average found. The mean scattered power density is plotted in (b) – (f). Initial modelling, (b) and (c), used a single angle of incident at 90° to the scale surface. (b) Scattered power density from a single elliptical bead with a 520 nm long axis and a 170 nm short axis with the long axis parallel to the incident radiation. (c) Scattered power plot when a 95 nm thick substrate is added 800nm below the centre of the single bead described above. This represents the lower substrate of the wing scale. More advance modelling, (d) – (f), used multiple angles of incidence to mimic diffuse illumination (d) Mean back scattered power density plot for the bead array models based described in Fig. 3(a), modelled with no base substrate. (e) Mean back scattered power density plot for the same bead-array models but including the 95 nm thick substrate situated 800 nm below the centre line of the beads. (f) Mean back scattered power density plot for the bead-array models including the base substrate and the UV absorption associated with the pterin pigmentation. Note. (b)-(c) and (d)-(f) are presented with different colour scales.

the scale structure (thereby reducing any near-field effects). The Poynting vector was then integrated over the 180 degrees above the scale structure to calculate the scattered power in the dorsal hemisphere.

The majority of previous work on the pierid butterflies has focussed on the absorption in the UV and on the optical scattering in the visible of the pterin beads themselves [19–21]. However, additional evidence has also been presented to suggest that beads are not solely responsible for optical scatter from the wing scales of white pierid butterflies. Giraldo and Stavenga observed a reduction in scatter of approximately 50% when all beads were removed [34]. This indicated a contribution of significant optical scatter from the remaining scale superstructure. Our detailed quantified bead removal experiments and subsequent optical scatter measurements agreed with this trend but not with the magnitude of reduction in scatter. We measured this reduction to be by a factor of 30%. Due to the importance, therefore, of scattering from non-bead intra-scale structures, detailed modelling of all intra-scale components was performed.

A significant increase in optical scattering into the hemisphere above the scale (dorsal hemisphere) was measured in the presence of the 95nm thick base substrate, compared to that associated with an isolated bead (Figs. 3(b) and (c)). The results presented are for a single incident angle of 90° although a similar scattering pattern was observed for a range of bead orientations and the full range of possible illumination angles. Integrating the scattered power density over the dorsal hemisphere indicated an average increase in scattered power, when the scale base substrate was included, of *ca.* 450% for wavelengths in the range 300-800 nm, compared to when the basal layer was omitted. For longer wavelengths ($\lambda > 600$ nm), when the scale basal layer was present, this increase in scattered power is as high as 800%. Analysis of the data suggests the scattering pattern observed (Fig. 3(b)), with peaks at a 90° angle and wavelengths of *ca.* 380 nm, 500 nm and 540 nm, is associated with a resonance within the 525 nm length of the bead. This combined with the base substrate reflectance peak at *ca.* 700 nm results in the enhanced scatter seen at 90° and above 600 nm in Fig. 3(c).

The disorder associated with the bead arrays on the wing scales appeared to enhance broadband scatter [21]. For our multi-bead array models, the effect of the presence of the basal layer was clearly demonstrated (Figs. 3(d) and (e)). Namely, scattered power density in the dorsal hemisphere was significantly increased when the scale substrate was included in the model. For this more realistic model, the integrated scattered power in the dorsal hemisphere increases by a mean value of approximately 350% when the scale substrate was included compared to when it was omitted (over a wavelength range of 300-800 nm). For these bead array models a full range of incident angles was used to mimic diffuse illumination. The key result of this modelling indicates that whilst the pterin beads enhance optical scatter from the scales, they are not solely responsible for it. The underlying scale structure, specifically the scale substrate, is also a vital component in the scattering system

The strong UV absorption [35] by the pterin pigment leucopterin was incorporated into the multi-bead models. By incorporating the absorption profile of leucopterin [16] in our multi-bead array model, including the scale substrate, a decrease of *ca.* 60% in absolute scattered power was observed for wavelengths below 420 nm (Fig. 3(f)). As expected, there is no significant change in the power scattered into the dorsal hemisphere for wavelengths longer than 420 nm where pterin absorption is negligible.

3.5 Characterisation of wing whiteness

The optical spectrophotometry and SEM measurements detailed in sections 3.1 and 3.2 were used to determine the dependence of wing reflectance on bead-array density. The same data may be applied further, using the analysis in section 2.4, in order to determine the dependence of actual wing colour quality on bead-array density. There is a statistically significant correlation between bead-array density and both brightness ($r^2 = 0.55$, $p < 0.001$) and CIELab L^* ($r^2 = 0.55$, $p < 0.001$) (Fig. 4(a)). Both brightness and CIELab L^* are a measure of how much light is scattered (reflected) over a certain visible wavelength range. Brightness is a measure of reflectance over the wavelength range of 457 ± 44 nm [28], whereas L^* is a measure of the reflectance over a wider range of approximately 400 - 700 nm

[28]. Therefore, the correlations between brightness, L^* bead-array density provide further understanding of the explicit optical scattering effect of pterin beads. This supports work of other studies that the pterin beads enhance optical scatter for wavelengths where absorption is negligible [18, 21, 33].

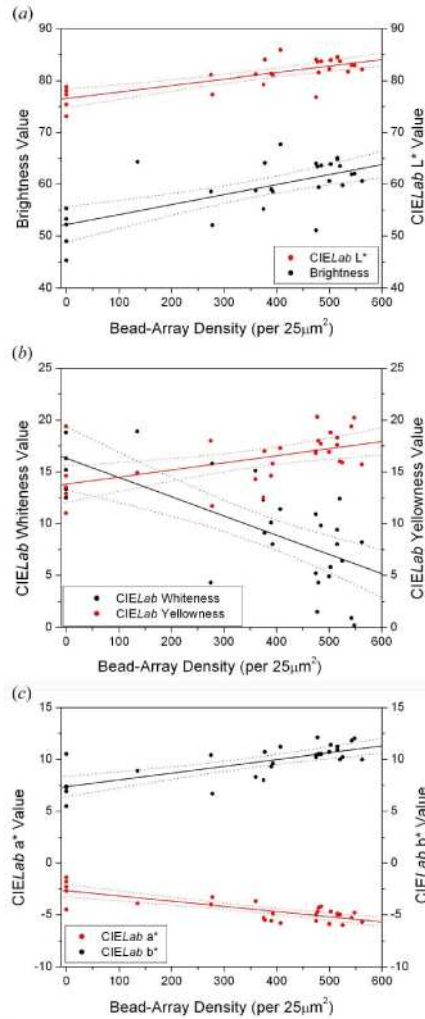


Fig. 4. Colour parameter plots for male *P. rapae* dorsal wings. (a) CIE Lab whiteness and yellowness as a function of pterin granule density. Reduced UV / blue absorption leads to an increase in whiteness and a reduction in yellowness. (b) Brightness and luminosity (L^*) of male *P. rapae* wings. Both brightness and luminosity drop as the scattering centres (pterin granules) are removed. (c) CIE Lab a^* and b^* colour coordinates. As pterin granule density decreases, both a^* and b^* tend towards zero, in line with the increase in whiteness.

The colour of the wing samples changed noticeably when the pterin beads were removed. Untreated wing samples had a distinct yellow tint. As the pterin beads were removed this tint decreased and the samples became noticeably whiter. This is confirmed by quantitative measurements of CIE Lab whiteness and yellowness (Fig. 4(b)). We observed a statistically significant trend in whiteness ($r^2 = 0.20$, $p = 0.0022$), and consistent yet not significant trend in yellowness ($r^2 = 0.59$, $p = 0.0713$). We suggest that the trend is not statistically significant due to the small sample size of approximately 20 and the variation of our natural samples. The

reason for these colour trends is well understood. Leucopterin, present in the wing samples has a UV absorption edge at *ca.* 450nm [16]. It therefore absorbs some short wavelength visible light, resulting in the distinct yellow tint and consequent low whiteness value. Removal of the leucopterin sees an increase in short wavelength reflectance; this reduces the yellow tint, thereby increasing the whiteness value.

The colour quality values calculated from the reflectance spectra of these wing samples is dependent on their colour coordinates a^* and b^* (see section 2.4). The b^* values (yellow-blue colour axis) are consistently positive, regardless of the extent of bead removal. This confirms by analysis what the human eye perceives; namely that the sample is tinted yellow at all bead array densities. However, Fig. 4(c) show a decrease in b^* value with increasing bead removal (i.e. lower bead-array density). A simple linear model suggests that bead-array density is significant in explaining its influence on b^* ($r^2 = 0.53$, $p < 0.001$). This demonstrates the relative increase in short-wavelength reflectance as the pterin beads are removed.

Similarly, the a^* value (green-red colour axis) is consistently negative, regardless of the extent of bead removal (Fig. 4(c)). Furthermore, it tends towards zero with decreasing bead-array density ($r^2 = 0.63$, $p < 0.001$). This indicates that there is a green tint on the wing, which is not readily discernable by the human eye, principally because the tint is dominated by the larger magnitude of b^* compared to a^* .

Both the a^* and b^* coordinates tend to zero with decreasing bead-array density. This explains the observed increase in the whiteness value with bead removal, because a high whiteness value requires both a^* and b^* to be close to zero.

4. Discussion

4.1 The effect of the pterin bead-array on scattering from the wing

P. rapae butterflies have deposits of UV absorbing pigment contained in nanoscale beads deposited throughout their wing scale surfaces. Previous studies [19, 21, 33] have shown that these beads enhance light scatter from their scales for wavelengths that they do not absorb, thus increasing overall reflectance at visible wavelengths. This understanding is strongly supported by our series of bead removal experiments and theoretical analyses. We found that controlled removal of the beads, via different immersion times of wing samples in ammonium hydroxide solutions (Fig. 2(a)) dramatically changes the UV-visible reflectance. Bead removal was found to increase UV reflectance significantly and simultaneously reduce longer wavelength reflectance (Fig. 2(b)).

Typical scale reflectances at visible wavelengths ($\lambda > 450$ nm) drop from *ca.* 68% for wing scales with a bead-array density of 21.0 ± 0.7 beads per square micron, to *ca.* 50% for scales from which all beads have been removed. This is a decrease in reflectance by a factor of one third, confirming the strong optical scattering role of the pterin beads.

This conclusion was further supported by the correlation observed between bead-array density and light scatter coefficient (Fig. 2(f)). Whilst previous studies have based their conclusions solely on reflectance data, we have measured the light scatter coefficient directly. These data directly imply that as the light scatter coefficient is non-zero when all beads are removed, the scale superstructure contributes significantly to the optical scatter observed. The scale structures were extensively modelled in this study, and the results indicate that the scale structure as a whole, and the lower scale substrate in particular, play a key role in producing a significant component of the broadband optical scatter. This conclusion holds when the inherent absorption associated with leucopterin pigmentation [16, 19, 36] is included in the model. This is to be expected since absorption by leucopterin is negligible for wavelengths above 450 nm.

The presented results contribute a further step toward fully understanding the scattering processes that underpin the appearance of pierid butterfly wing scales. However, their wing scale reflectances cannot be fully understood from the optics and analysis of a single scale

because the scales are layered in overlapping rows on each wing substrate [21, 37]. Scattered light will contain a contribution from all high/low refractive index interfaces; therefore a full model comprising all components of the wing structure would be required to gain complete understanding of the scattering processes responsible for wing colouration. Both Stavenga *et al.* [37] and Yoshioka & Kinoshita [38] used simplified multi-layer structures to model the stacking of scales on a butterfly wing. A combination of these multilayer techniques and the individual scale modelling discussed here would create an accurate wing model and allow further understanding of the optical scatter from the wing.

4.2 The effect of pterin bead presence on wing colour quality

Analysis of the data collected in this investigation clearly shows that the presence of pterin pigments has a marked effect on the wing colour quality of the *P. rapae* butterfly. As the pterin bead-array density is reduced, there is a significant rise in the numerical whiteness value of the wings. The numerical whiteness is the industry standard whiteness value calculated using the CIE*Lab* L^* , a^* and b^* values. The increase in CIE*Lab* whiteness occurs despite an overall reduction in scattered intensity due to the lower bead array density. This is because it is the shape of the reflectance profile, not its intensity, which dictates the whiteness value [28]. The trends in the yellowness value (Fig. 2(a)), L^* (Fig. 2(b)), a^* and b^* (Fig. 2(c)) add further support to the hypothesis that pterin beads significantly affect not only the intensity of optical scatter, but also wing colour quality.

The colour coordinate data associated with a^* and b^* provide further insight into which pterins may be present in these *P. rapae* wing samples. Wings not treated in ammonium hydroxide solution have a visibly yellow tint to their whiteness. This results in the relatively large positive b^* value measured. The yellowness is caused by the absorption of short wavelength ($\lambda < 450$ nm) light by the pterin beads. Absorption spectra from purified pterin samples and those derived from wing reflectance of many pierid butterflies [16], including *P. rapae crucivora*; suggest that the main pterin present in white pierid butterflies is leucopterin, although xanthopterin may also be present. Our correlation between bead array density and brightness (Fig. 4(b)) indicates that the presence of xanthopterin is unlikely. The absorption edge of xanthopterin lies at approximately 450 nm, which is in the middle of the wavelength band (457 ± 44 nm) measured to calculate brightness [28, 39]. The presence of xanthopterin would therefore suppress wing brightness, and removal of the xanthopterin would lead to a measurable increase in brightness, despite the loss of the pterin beads as scattering centres. However, our brightness data (Fig. 4(b)) indicates that this is not the case. The brightness of the wing samples is seen to decrease as the scattering centres (pterin beads) are removed. We conclude, therefore, that xanthopterin is not present in wing of male *P. rapae*.

4.3 Biological implications of pterin bead array density

Significant research has been conducted on the mating habits of pierid butterflies. Obara [40] and Rutowski [41] suggest that UV absorption by the wings is crucial in distinguishing between males and females. This is particularly the case for *P. r. crucivora* where there is a distinct sexual dimorphism [23]. This dimorphism is not so distinct for British *P. rapae* species, of which the wing scales of both male and female are adorned with beads and subsequently exhibit low UV reflectance [33]. We found that males typically have a wing scale bead-array density of $21 \pm 2 \mu\text{m}^{-2}$ (sample size = 40) whereas females have a lower bead-array density of $14.5 \pm 0.5 \mu\text{m}^{-2}$ (sample size = 10). Only at longer, visible wavelengths do the magnitudes of the reflectances significantly differ between males and females. Obara & Majerus conducted experiments on British *P. r. rapae* and observed that the lack of distinct sexual dimorphism occasionally leads to males approaching other males mistakenly in courtship [24]. They also showed that it is the female wings, not the female body that elicits the mating response in male *P. r. rapae*.

Rutowski *et al.* [20] and Kemp *et al.* [22] suggest that the UV reflectance generated by wing scales in the butterfly *C. eurytheme* contains information about the quality of the lamellae-based nanostructure that generates the signal giving an honest indication of the condition of the male butterfly. The contrast in reflectance of short wavelengths ($\lambda < 430$ nm) to that of the longer wavelength region from male *P. rapae* wings is directly correlated with the wing scale pterin bead array-density (Fig. 2(b) inset). This may give a similar indication of the fitness of the individual, but this would need to be confirmed by behavioural studies.

Little is known about the cost imposed by the presence of dense pterin bead-arrays and whether pterin based colour variation might itself encode information about fitness or quality [19]. In the case of *P. rapae* studied here, the signal comprises two components; reflectance from a highly scattering scale structure, combined with a highly wavelength-selective absorbing pigment. Males that are unable to deposit adequate amounts of pterin may be disadvantaged when attempting courtship, as the poor UV-visible contrast from their wings may indicate that the male is of low quality [20]. This disadvantage may be significantly enhanced for British *P. r. rapae* males, where a low pterin bead-array density, more similar to those of British *P. r. rapae* females, could potentially lead to a male becoming less visually distinguishable from females. We conclude that, as with other animal species, the sexual dimorphism in colour appearance may enhance sexual recognition in pierid butterflies. This is in broad agreement with previous studies on the matter [19, 21, 33, 41].

5. Conclusion

We have shown that the wing scales of male *P. rapae* are adorned with a dense array of microscopic elliptical beads, and built upon previous work suggesting that these beads were responsible for both enhancing optical scatter and significant absorption at UV wavelengths. Kubelka-Munk theory, a theory based on how light is reflected and transmitted in thin layers [28], was used to calculate the scattering coefficient of the wing samples; it is apparent that there is a positive correlation between scattering coefficient and pterin bead-array density. It was observed that the scattering coefficient did not tend to zero when all pterin beads were removed, suggesting that some other scale structure was responsible for some of the optical scatter observed. Finite element modelling of all components of the scale structure highlighted that the scale substrate in particular is critical in effecting the significant optical scatter observed in our reflectance spectra. Specialisation of scales on certain regions of the wing were also observed, the black spots were found to contain no pterin beads [21] (unpublished data) but maintained the general scale superstructure. We conclude that localised pigmentation of the scale structure must be responsible for the difference in observed reflectance between white and black wing regions. Note however, that the pigmentation of black scales is largely melanin [42] and is unrelated to the pterin pigments contained within the bead-array of the white scales. A detailed colour analysis of wing samples with varying bead-array densities revealed that both optical scatter from the pterin bead-array and absorption by the pterin pigments themselves dictate the final colour appearance of the *P. rapae* wing. Our experimental data and the resulting optical scatter and colour analyses indicate that the wing scale pterin bead-array enhances optical scatter whilst simultaneously absorbing UV wavelengths, in line with previous work on the matter.

Acknowledgements

We thank C. M. Luke for help with the statistical modelling and Prof. D Stavenga for constructive criticism of an early draft. Great Western Research (GWR) and the School of Physics at The University of Exeter supported this work.